

Efficiency and Mechanism of heat flux rectification with non-reciprocal surface waves in Weyl-Semi-Metals

A. Naeimi and S.-A. Biehs

Institut für Physik, Carl von Ossietzky Universität, 26111, Oldenburg, Germany

(Dated: December 16, 2024)

We investigate the mechanism of near-field heat transfer rectification between two Weyl semimetal nanoparticles and a planar Weyl semimetal substrate via the coupling to non-reciprocal surface modes. We show that depending on the distance between the nanoparticles there can be a heat flux rectification with ratios of about 6000 which are much higher than previously predicted rectification ratio of 2673. Furthermore, we identify a previously overlooked range of forward rectification and a range of strong backward rectification with rectification ratios larger than 8000 for relatively small Weyl node separations. We investigate the mechanism behind this large heat flux rectification.

I. INTRODUCTION

Different thermal rectification mechanisms for heat radiation in the nanoscale regime have been studied which of course also, in general, work in far-field setups. One mechanism is to use the intrinsic temperature dependence of the material properties of the involved materials [1–4] which can lead to a very large heat flux rectification, i.e. a diode-like effect, when the involved elements undergo a phase transition as superconductors [5, 6] or phase change materials like VO_2 as studied theoretically and experimentally in Refs. [7–10]. Such diode like elements can also function as thermal transistors for heat radiation [11] as experimentally verified in a far-field setup [12]. Interestingly, also asymmetric many-body systems can show a thermal rectification [13].

Another possibility to achieve thermal rectification for heat radiation is to employ magneto-optical materials which have a non-reciprocal material response when an external magnetic field is applied. This non-reciprocal property results in interesting properties of near- and far-field thermal radiation. For example it could be shown that in thermal equilibrium there is a persistent heat current [14], spin and angular momentum [15, 16], a Hall effect for heat radiation [17], spin-directional thermal emission [18], a giant magneto-resistance [19, 20], a Berry phase of thermal radiation [21] as well as a non-reciprocal version of the Green-Kubo relation [22]. Also the impact on the heat radiation between planar films and multilayers with an applied magnetic field has been studied [23–25] as well as the heat flux between a magneto-optical nanoparticle and planar substrate [26]. Finally, the coupling to non-reciprocal surface modes allows for a strong heat flux rectification [27] due to the spin-spin coupling [28] to the non-reciprocal surface waves which are spin-momentum locked [29, 30]. All those works show that the magnetic field provides a mean to control the magnitude and direction of the radiative heat flux actively (see also reviews [31, 32]).

The existence of intrinsically non-reciprocal materials such as the Weyl semimetals (WSM) [33, 34] allows to realize the same effects as found for magneto-optical materials but without the need of an externally applied mag-

netic field. Consequently, it could be shown that there is a photonic spin hall effect [35], an anomalous Hall effect for thermal radiation [36], modulated heat transfer between slabs and multilayers [37–41], negative differential thermal conductance [42], the possibility to enable thermal routing [43], non-reciprocal absorption and emission [44, 45], broadband circularly polarized thermal radiation [46], non-reciprocal farfield heat radiation [47], and coupling to graphene nanoribbons [48]. These and other effects are reviewed in Ref. [49, 50], for instance. Of course, there is also a thermal rectification due to the coupling to non-reciprocal surface [51]. The heat flux rectification is predicted to be more efficient for WSM than for magneto-optical materials like InSb [51].

The aim of our work is to provide a detailed study of the thermal rectification of the heat flux between two WSM nanoparticles by the interaction with the non-reciprocal surface waves of a close by planar WSM sample as sketched in Fig. 1 and first studied for InSb in Refs. [27, 28] and for WSM in Ref. [51]. We explain the underlying mechanism on the basis of the properties of the involved surface modes and show that the thermal rectification can be much higher than the predicted rectification ratio of 2673 in the original work [51]. Furthermore, we show that a regime of high rectification for small values of the Weyl node separation has been overlooked previously, which can easily lead to rectification ratios of about 8000.

II. NEAR-FIELD RADIATIVE HEAT TRANSFER

Within the framework of fluctuational electrodynamics the radiative heat flux between dipolar objects each at local thermal equilibrium has been studied intensively and general expressions for the mean power received by each dipolar object have been derived [31]. Considering only two dipolar objects having local equilibrium temperatures T_1 and $T_2 < T_1$ in close vicinity to an interface at temperature $T_s = T_2$ (see forward case in Fig. 1) the

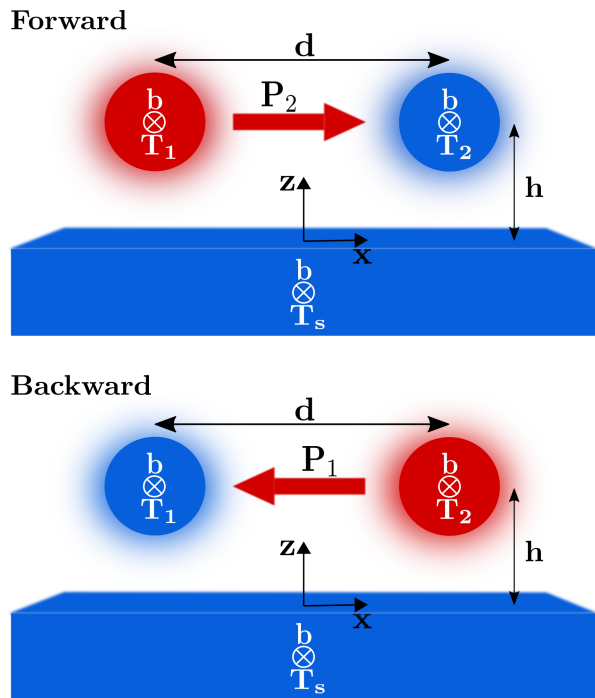


Figure 1: Sketch of our physical system consisting of two spherical nanoparticles with Radius R and temperatures T_1 , T_2 placed at $-d/2$ and $d/2$ in a height h above a planar substrate. The substrate and the nanoparticles are made of the same WSM and the temperature of the substrate is at temperature T_s . In the forward case $T_1 > T_2$ and $T_s = T_2$ whereas in the backward case $T_2 > T_1$ and $T_s = T_1$. The Weyl node separation $\mathbf{b} = b\hat{y}$ is aligned in positive y direction.

power P_2 received by object 2 has the general form [31]

$$P_2 = 3 \int_0^\infty \frac{d\omega}{2\pi} \hbar \omega n_1 \mathcal{T}_{12} \quad (1)$$

with the mean photon number $n_1 = (e^{\hbar\omega/k_B T_1} - 1)^{-1}$, a transmission coefficient \mathcal{T}_{12} , and Planck's reduced constant \hbar . In the reverse scenario where $T_2 > T_1$ and $T_s = T_1$ (see backward case in Fig. 1) the power P_1 received by object 1 has the general form

$$P_1 = 3 \int_0^\infty \frac{d\omega}{2\pi} \hbar \omega n_2 \mathcal{T}_{21}. \quad (2)$$

with mean photon number $n_2 = (e^{\hbar\omega/k_B T_2} - 1)^{-1}$ and a transmission coefficient \mathcal{T}_{21} . In the single scattering limit the transmission coefficients are given by simple trace formulas ($i, j = 1, 2$) [31]

$$\mathcal{T}_{ij} = \frac{4}{3} k_0^4 \text{Tr} [\chi_j \mathbf{G}(\mathbf{r}_j, \mathbf{r}_i) \chi_i \mathbf{G}^\dagger(\mathbf{r}_j, \mathbf{r}_i)]. \quad (3)$$

In these expressions for both transmission coefficients the Green function $\mathbf{G}(\mathbf{r}_j, \mathbf{r}_i)$ contains the whole information about the environment. In our case the Green function consists of the vacuum and a scattering part due to the

presence of a substrate. For a planar non-reciprocal semi-infinite substrate the explicit expressions for the Green function can be found in Ref. [27, 51], for instance. Now, the properties of the two dipolar objects enter into the transmission coefficient by

$$\chi_i \approx \frac{1}{2i} (\alpha_i - \alpha_i^\dagger) \quad (4)$$

where α_i is the polarizability tensor of the dipolar object. Note, that here we neglect the radiation correction which is typically small in the infrared regime. Obviously, the non-hermitian part of the polarizability of the two objects determines the heat transfer between the objects. For spherical nanoparticles with radii $R_1 = R_2 \equiv R$ as discussed here, the polarizabilities are given in terms of the particles permittivity tensors ϵ_i ($i = 1, 2$) as [31]

$$\alpha_i = 4\pi R^3 (\epsilon_i - 1) (\epsilon_i + 2\mathbf{1})^{-1} \quad (5)$$

In the following we will use the above approximate expressions for the numerical evaluation of the radiative heat transfer in order to have comparable results to Ref. [51] where the same approximations have been used. The goal is to study the heat transfer between the nanoparticles via the surface waves of a nearby interface [52–58] but with the specificity that the surface waves are non-reciprocal [27, 28]. We finally emphasize that the dipolar approximation only holds when the distance between the dipolar objects and the interface are sufficiently large. As a rule of thumb a center-to-center (center-to-surface distance) of $4R$ ($3R$) is sufficient to guarantee the validity of the dipolar approximation [59–61].

III. PERMITTIVITY OF WSM

Our main focus is on the radiative heat transfer between WSM nanoparticles due to the coupling to non-reciprocal surface modes in a close by substrate of the same WSM. For these materials the permittivity tensor is non-reciprocal, i.e. $\epsilon \neq \epsilon^t$. Assuming that the vector connecting the Weyl nodes in k -space is pointing in y -direction and the WSM possess no chiral magnetic effect, the permittivity tensor is

$$\epsilon(T, \omega) = \begin{pmatrix} \epsilon_d & 0 & i\epsilon_a \\ 0 & \epsilon_d & 0 \\ -i\epsilon_a & 0 & \epsilon_d \end{pmatrix}. \quad (6)$$

In a generally accepted simplified model the diagonal and non-diagonal elements are [34]

$$\epsilon_a(\omega) = \frac{be^2}{2\pi^2 \epsilon_0 \hbar \omega} \quad (7)$$

and

$$\begin{aligned} \epsilon_d(\omega, T) = & \epsilon_b + i \frac{r_s g_w \Omega}{6\Omega_0} G\left(\frac{\Omega}{2}\right) \\ & - \frac{r_s g_w}{6\pi\Omega_0} \left\{ \frac{4}{\Omega} \left[1 + \frac{\pi^2}{3} \left(\frac{k_B T}{E_F} \right)^2 \right] \right. \\ & \left. + 8\Omega \int_0^{\eta_c} d\eta \eta \frac{G(\eta) - G(\Omega/2)}{\Omega^2 - 4\eta^2} \right\}. \end{aligned} \quad (8)$$

Here we have introduced the general quantities like the permittivity of vacuum ϵ_0 and the model and material de-

pendent quantities $\Omega = \hbar(\omega + i\tau^{-1})/E_F$, $\Omega_0 = \hbar\omega/E_F$, $r_s = e^2/(4\pi\epsilon_0\hbar v_F)$, the Fermi energy E_F , the Fermi velocity v_F , the number of Weyl nodes g_w , the separation of the Weyl nodes $2b$, the cutoff energy E_c and $\eta_c = E_c/E_F$. Finally, we also have $G(E) = n(-E) - n(E)$ where $n(E)$ is the Fermi distribution function. As material parameters we use $g_w = 2$, $\epsilon_b = 6.2$, $v_F = 0.83 \times 10^5$ m/s, $\tau = 10^{-12}$ s, $b = 2 \times 10^9$ m $^{-1}$, $\eta_c = 3$ and the temperature dependent Fermi energy

$$E_F(T) = \frac{2^{1/3} \left[9E_F(0)^3 + \sqrt{81E_F(0)^6 + 12\pi^6 k_B^6 T^6} \right]^{2/3} - 2\pi^2 3^{1/3} k_B^2 T^2}{6^{2/3} \left[9E_F(0)^3 + \sqrt{81E_F(0)^6 + 12\pi^6 k_B^6 T^6} \right]^{1/3}} \quad (9)$$

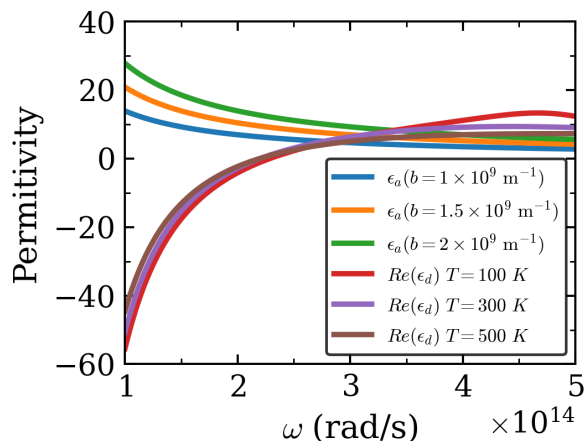


Figure 2: The permittivity tensor components ϵ_a and ϵ_d of the WSM as function of frequency. For the non-diagonal elements b is varied whereas for the diagonal components we vary the temperature.

with $E_F(0K) = 0.163$ eV so that $E_F(300K) = 0.15$ eV. This choice of parameters is the same as in Ref. [51] and corresponds to materials like Co_3MnGa and Co_2MnGa [38]. A similar choice of parameters but with $b = 8.5 \times 10^8$ m $^{-1}$ corresponds to $\text{Co}_3\text{Sn}_2\text{S}_2$ [41].

In Fig. 2 we show the diagonal and non-diagonal components of the permittivity for different temperatures and different values of the Weyl node separation b . We therewith reproduce the same results as in Ref. [51]. It can be observed that the non-diagonal elements are very sensitive to a change in b whereas the diagonal elements depend on temperature only.

IV. LOCALIZED SURFACE MODES AND NON-RECIPROCAL SURFACE WAVES IN WEYL-SEMI-METALS

The heat or energy transfer between the particles is due to a coupling of the localized resonances in the particle with the surface mode resonances of the planar substrate. The localized resonances of the nanoparticles are determined by the poles of the polarizability and here we obtain as for magneto-optical materials with applied magnetic field three dipolar resonances with magnetic quantum numbers $m = 0, \pm 1$ defined by

$$\epsilon_d(\omega_{m=0}) = -2 \quad (10)$$

and

$$\epsilon_d(\omega_{m=\pm 1}) = -2 \mp \epsilon_a(\omega_{m=\pm 1}). \quad (11)$$

Obviously, the non-diagonal elements induce a Zeeman-like splitting [15, 62] linear in ϵ_a and therefore linear in the Weyl node separation b whereas the resonance frequency $\omega_{m=0}$ does not depend on b . In table I we list some numerical results for the resonance frequencies for different temperatures and Weyl node separations. Due to the obvious analogy of the analytical expressions, one can find for the WSM non-vanishing spin, angular momentum and a circular heat flux for the resonance $\omega_{m=\pm 1}$ as discussed for magneto-optical materials in Ref. [15, 32]. Due to the temperature dependence of the diagonal elements of the permittivity tensor of the WSM the exact spectral position of the resonance frequencies will depend not only on b but also on the temperature of the nanoparticles.

On the other hand, the interface of the planar WSM will support surface waves which are non-reciprocal and have similar properties as the non-reciprocal surface

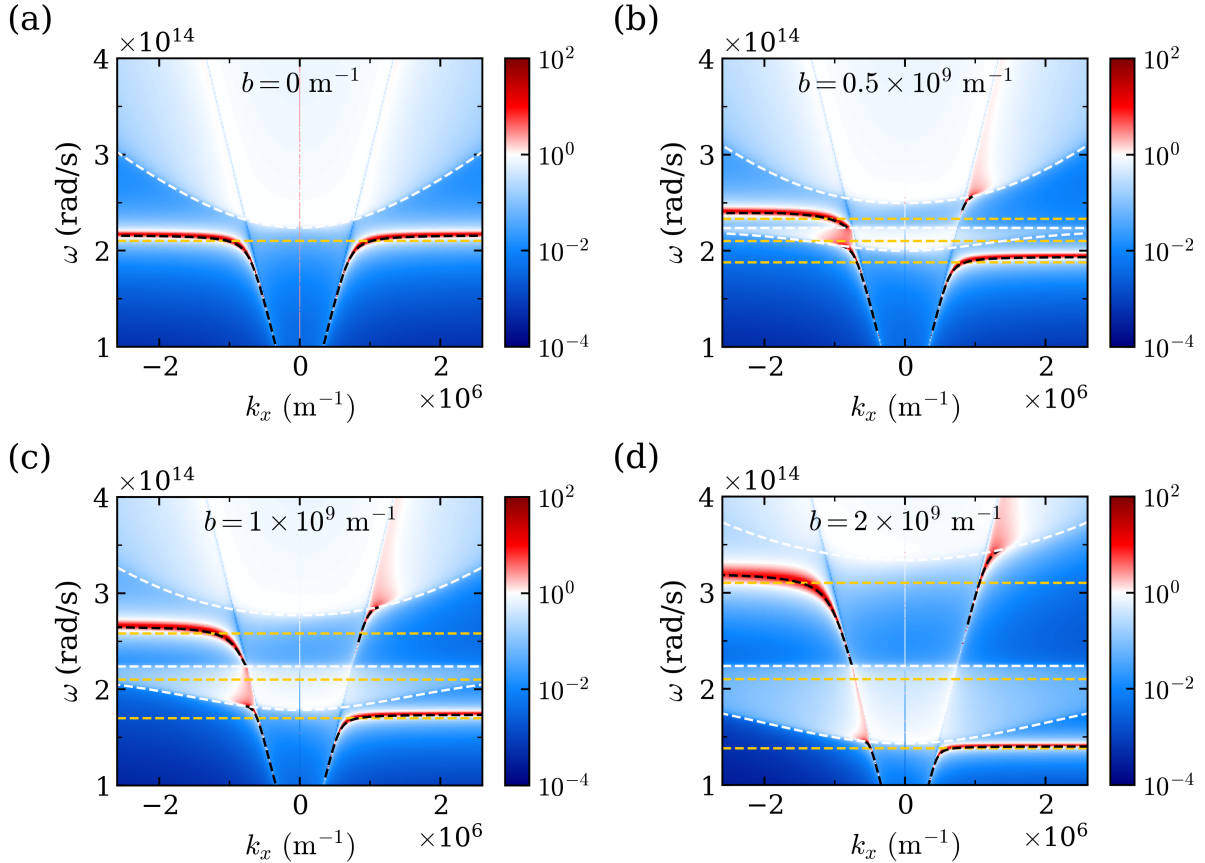


Figure 3: Reflection coefficient for p-polarized light r_{pp} of Weyl material for the Voigt configuration in ω - k_x plane for different values of $b = 0, 0.5 \times 10^9, 1 \times 10^9, 2 \times 10^9 \text{ m}^{-1}$ for $T_s = 180 \text{ K}$. For propagating waves with $|k_x| \leq k_0$ the quantity $1 - |r_{pp}|^2$ is shown and for evanescent waves with $|k_x| > k_0$ the quantity $\text{Im}(r_{pp})$ is plotted. The black dashed lines are the dispersion relations of the surface modes from Eq. (12). The white lines are the light lines defined by $k_x = k_0 \sqrt{\epsilon_V}$. The horizontal dashed orange lines mark the frequencies of the resonances $\omega_{m=0,\pm 1}$ of the nanoparticles determined from Eq. (11).

T (K)	b (10^9 m^{-1})	$\omega_{m=0}$ (10^{14} rad/s)	$\omega_{m=+1}$ (10^{14} rad/s)	$\omega_{m=-1}$ (10^{14} rad/s)
200	2	2.08	1.36	3.08
180	2	2.09	1.37	3.08
180	0.5	2.09	1.88	2.3
180	0.19	2.091	2.008	2.176

Table I: Numerical values of the nanoparticle resonance frequencies $\omega_{m=0,\pm 1}$ for particle temperatures of 180 K and 200 K and different values of the Weyl node separation.

waves in magneto-optical materials with applied magnetic field [34, 63]. For these non-reciprocal surface waves general expressions for the dispersion relation can be derived [64–66]. Here we are mainly interested in the propagation of the surface waves in $\pm x$ direction assuming a Voigt configuration, i.e. an applied magnetic field or Weyl node vector perpendicular to the x - z plane spanned by the nanoparticles and the surface. In that case ($k_y = 0$) the surface wave dispersion relation can be simplified

to [66]

$$k_x^2 - k_0^2 \epsilon_d - k_z k_x^V \epsilon_d - k_z k_x i \epsilon_a = 0 \quad (12)$$

with the wavevectors $k_z = \sqrt{k_0^2 - k_x^2}$, $k_z^V = \sqrt{k_0^2 \epsilon_V - k_x^2}$ and the Voigt permittivity $\epsilon_V = (\epsilon_d^2 - \epsilon_a^2) / \epsilon_d$. To determine the corresponding k_x and ω values of the dispersion relation of surface modes we determine real valued solutions k_x for real frequencies. This can be done when neglecting dissipation in the material. On the other hand, to determine the propagation length we determine the complex valued solutions of k_x for real frequencies. In this case, the dissipation inside the material is included. Then we can define the surface propagation length in a standard way by [28]

$$\Lambda_{\pm} = \frac{1}{2\text{Im}(k_x^{\pm})} \quad (13)$$

where k_x^{\pm} is the complex solution of the dispersion relation for waves travelling in $\pm x$ direction.

In Fig. 3 we show $1 - |r_{pp}|^2$ for the propagating waves with $|k_x| < k_0$ and $\text{Im}(r_{pp})$ the evanescent waves with

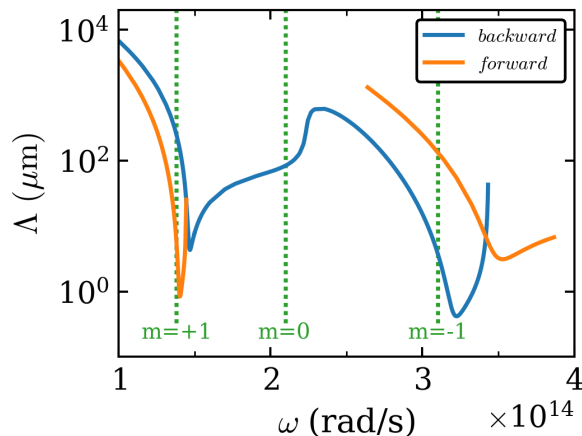


Figure 4: Propagation length Λ_{\pm} from Eq. (13) for the Weyl point separation $b = 2 \times 10^9 \text{ m}^{-1}$. Vertical lines mark the positions of the localized particle resonances.

$|k_x| > k_0$ using the expressions for the reflection coefficient for anisotropic media from Ref. [67]. The plotted quantities in the $\omega - k_x$ plane are essentially proportional to the photonic density of states. The different surface wave modes in the evanescent sector $|k_x| > k_0$ with large values for $\text{Im}(r_{pp})$ can be nicely seen as well as the Zeeman splitting of surface waves travelling towards $\pm x$ direction for non-zero Weyl node separation $b \neq 0$. For $b = 0$ there is no non-reciprocity and the three dipolar resonances as well as the surface mode resonances are degenerate. This effect of the splitting of the surface waves is the same as for magneto-optical surface waves when a magnetic field is applied [27, 34, 63–66] so that the Weyl node separation $\mathbf{b} = b\hat{y}$ plays the same role as the magnetic field $\mathbf{B} = B\hat{y}$. It should be noted that the dispersion relations of the surface modes shown in Fig. 3 are determined by neglecting losses in order to avoid backbending effects, whereas the reflection coefficients are evaluated with taking dissipation into account. By comparing the dispersion relations obtained from Eq. (12) with the reflection coefficients it can be seen that with dissipation the surface modes can exist at frequencies which are forbidden in the case without dissipation, i.e. in the region between the white dashed Voigt lightlines defined by $k_x = k_0\sqrt{\epsilon_V}$. In particular, there are surface modes travelling in negative x direction in the frequency band between the two Zeeman splitted surface modes. Furthermore, we have plotted in Fig. 3 the frequencies of the localized dipolar resonances within the nanoparticles. From this representation it can be seen which particle resonances can couple to the surface waves in $\pm x$ direction. This feature will be essential to understand the rectification mechanism for the radiative heat transfer.

In Fig. 4 we show the propagation length Λ_{\pm} of the surface waves traveling in $\pm x$ obtained from Eq. (13) for $b = 2 \times 10^9 \text{ m}^{-1}$ with losses included. As can already

be seen in Fig. 3(d) the localized resonance at $\omega_{m=0}$ can only couple to surface waves travelling in $-x$ direction, because there are no surface wave solutions for surface waves travelling in $+x$ direction for this frequency. On the other hand, the resonances $\omega_{m=\pm 1}$ can couple to surface waves travelling in both $\pm x$ direction but with the difference that the propagation length is dependent on the propagation direction. At $\omega_{m=+1}$ the excited surface waves in $-x$ direction travel farther than those in $+x$ direction and at $\omega_{m=-1}$ it is the opposite trend. From this observation one can expect that for large enough inter-particle distance d the backward heat flow is preferred at $\omega_{m=+1}$ and a forward heat flow at $\omega_{m=-1}$.

V. HEAT FLUX RECTIFICATION

The heat flux rectification between the nanoparticles can be quantified by the rectification ratio [51]

$$\eta = \frac{P_1 - P_2}{P_2} \quad (14)$$

which by definition can be larger than one. In some works like Ref. [7] normalized rectification ratios are used. This definition is useful when the heat flow is enhanced in backward direction. In the opposite case when the heat flux is enhanced in forward direction then it is better to use the rectification ratio

$$\tilde{\eta} = \frac{P_2 - P_1}{P_1} \quad (15)$$

correspondingly.

In Fig. 5 we show the numerical results for P_1 and P_2 in the backward and forward scenario together with the rectification ratio η for two WSM nanoparticles of Radius $R = 20 \text{ nm}$ at a distance of $h = 100 \text{ nm}$ above a WSM substrate as a function of the Weyl node separation b . We chose $T_1 = 200 \text{ K}$, $T_2 = T_s = 180 \text{ K}$ for the forward and vice versa for the backward case. It can be seen that there are for the shown distances in general two maxima for the power P_1 and P_2 as well as for the rectification ratio. The location of the maxima depends on the distance d . We note that for values of b smaller than 10^8 m^{-1} the power P_2 for the forward case is larger than P_1 for the backward case. This means that a heat flux in forward direction is preferred and therefore this rectification can hardly be seen in the rectification ratio η but in $\tilde{\eta}$ which can have values up to 15 for the studied distances [see inset of Fig. 5(b)]. This rectification in forward direction is small compared to the strong rectification in backward direction for larger values of b as can be nicely seen in Fig. 5(b). The first rectification maximum for small b can be as large as about 8000 and the second rectification maximum at larger values of b can be as large as about 6000 for $d = 2000 \text{ nm}$.

In order to understand the physical mechanism leading to the large rectification in backward direction for two

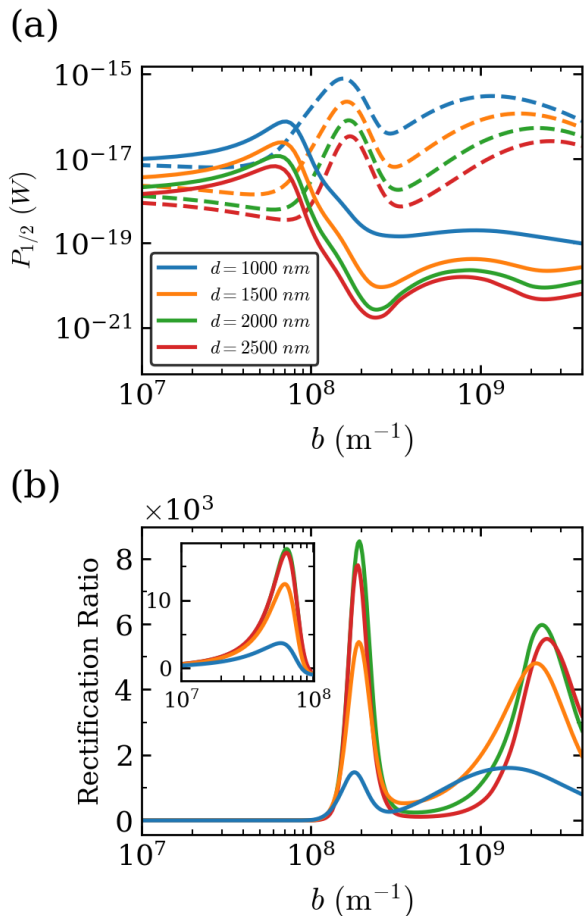


Figure 5: (a) P_2 (solid line) and P_1 (dashed line) and (b) Rectification ratio η from Eq. (14) between two WSM nanoparticles of Radius $R = 20$ nm above a WSM substrate at a height of $h = 100$ nm as a function of the Weyl node separation for different interparticle distance $d = 1000$ nm, 1500 nm, 2000 nm, and 2500 nm. Inset: Rectification ratio $\tilde{\eta}$ from Eq. (15) for the forward rectification.

distinct values of b we study in more detail the transmission coefficients \mathcal{T}_{12} and \mathcal{T}_{21} introduced for the forward and backward case in Eq. (3). In Fig. 6 we show both transmission coefficients choosing the interparticle separation distance $d = 1500$ nm for $b = 0.19 \times 10^9 \text{ m}^{-1}$ and $b = 2 \times 10^9 \text{ m}^{-1}$, i.e. for those values of the Weyl node separation where we find a maximal rectification ratio in Fig. 5. It can be nicely seen that there are three peaks due to the localized resonances within the nanoparticles corresponding to the resonance frequencies $\omega_{m=0,\pm 1}$ for the given value of b . For $b = 0.19 \times 10^9 \text{ m}^{-1}$ the transmission coefficient is in the backward direction larger than in the forward direction at all three resonances. On the other hand, for $b = 2 \times 10^9 \text{ m}^{-1}$ the two low frequency resonances are enhanced in the backward direction, whereas the high frequency resonance is enhanced for the forward direction.

Assuming that the rectification is due to the heat ex-

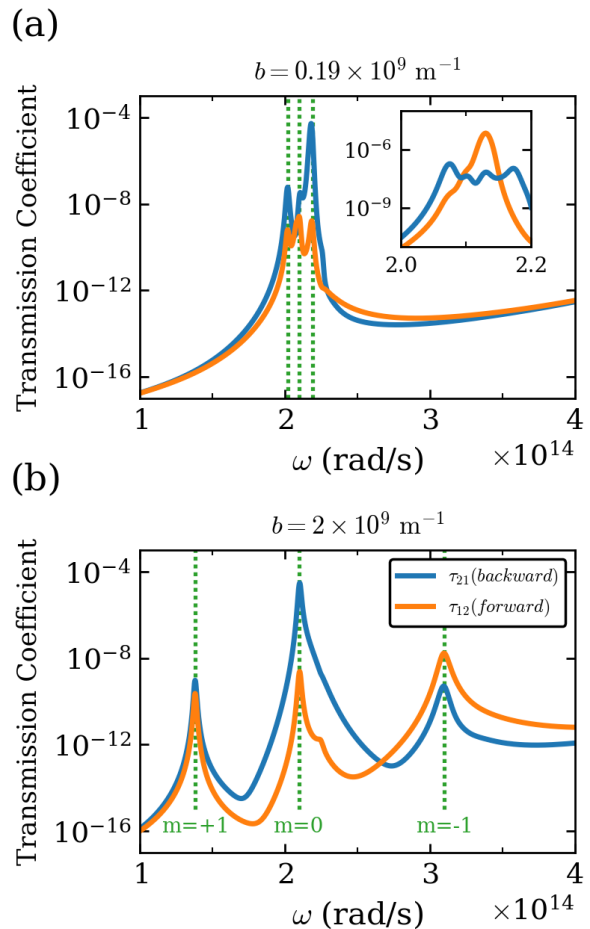


Figure 6: Transmission coefficients \mathcal{T}_{12} and \mathcal{T}_{21} for the backward and forward case for $d = 1500$ nm for (a) $b = 0.19 \times 10^9 \text{ m}^{-1}$ and $b = 2 \times 10^9 \text{ m}^{-1}$. The dashed lines indicate the spectral positions of the particle resonances. Inset: \mathcal{T}_{12} and \mathcal{T}_{21} for $b = 6 \times 10^7 \text{ m}^{-1}$.

change between the nanoparticles via the coupling to the surface modes, this behaviour can be explained by the properties of the surface modes. From the reflection coefficient in Fig. 3(a) and (b) it becomes obvious that for relatively small values of b the Zeeman-like splitting is relatively small. Actually, for very small $b < 10^8 \text{ m}^{-1}$ the particle resonance can couple to the surface modes in forward, i.e. $+x$ direction. This leads to a rectification in forward direction as can be seen in the curves of P_2 in Fig. 5(a) and the transmission coefficients in the inset of Fig. 6(a). For $b > 10^8 \text{ m}^{-1}$ a gap opens between the upper and lower bands of surface mode solutions as demonstrated in the reflection coefficient in Fig. 3(b). Due to this fact, the two high frequency particle resonances cannot anymore couple to surface modes in forward direction so that P_2 decreases for $b > 10^8 \text{ m}^{-1}$. In contrast, there are still surface modes in backward direction to which the nanoparticles can couple so that P_1 is generally larger than P_2 for $b > 10^8 \text{ m}^{-1}$. In particular

for $b = 0.19 \times 10^9 \text{ m}^{-1}$ there is a maximum in P_1 . This enhancement in the backward direction as also observed in the transmission coefficient in Fig. 6 (a) showing that all three particle resonances can efficiently couple to the surface modes in backward direction whereas only the low frequency resonance can couple to surface modes in forward direction.

A similar reasoning can be made for $b = 2 \times 10^9 \text{ m}^{-1}$. From the reflection coefficient in Fig. 3(d) it is apparent that the low frequency resonance couples similarly to the surface wave in both direction as for $b = 0.19 \times 10^9 \text{ m}^{-1}$ so that one can expect that the backward direction is slightly enhanced. This can also be seen in the transmission coefficient in Fig. 6(b). Now, the middle nanoparticle resonance for $m = 0$ can only couple to surface waves in $-x$ direction explaining the enhanced transmission in backward direction. Finally, the high frequency nanoparticle resonance can now couple to surface waves in both direction which is in contrast to the case of $b = 0.19 \times 10^9 \text{ m}^{-1}$. From the propagation length in Fig. 4(b) we found that the propagation length is higher in backward direction for the resonance at $\omega_{m=+1}$ and higher in forward direction for the resonance at $\omega_{m=-1}$. This feature explains the larger transmission coefficient at $\omega_{m=+1}$ in backward direction and the larger transmission coefficient in forward direction at $\omega_{m=-1}$. The fact, that for $b = 0.19 \times 10^9 \text{ m}^{-1}$ all nanoparticle resonances are enhanced in backward direction but for $b = 2 \times 10^9 \text{ m}^{-1}$ only the two low frequency resonances explains why the rectification maximum is higher for lower values of b .

For very large $b \gg 10^9 \text{ m}^{-1}$ the resonances $\omega_{m=\pm 1}$ move out of the spectral window determined by the Planck function so that in this case one might expect that there remains the rectification due to the coupling of the resonance at $\omega_{m=0}$ to the surface modes in backward direction. Therefore, the rectification tends to zero without changing its sign for large values of b in contrast to what was found for magneto-optical materials for large magnetic fields where the rectification changes its sign for large magnetic fields. Of course, one can also argue that we have a similar effect of changing the direction of rectification at relatively low b around 10^{-8} m^{-1} .

Finally, one can of course change the direction of rectification by turning the sample by 180° such that the orientation of the weyl nodes is in the particles in $+y$ direction and in the sample in $-y$ direction. However, the coupling strength between the surface modes and the particle resonances is reduces in this case so that the rectication changes its sign, but the rectification ratio is reduced as well as can be seen in Fig. 7. The general features seen in the rectification ratio remain the same. In Fig. 8 we show the variation of the rectification ratios as function of distance for $b = 2 \times 10^8 \text{ m}^{-1}$ and $b = 2 \times 10^9 \text{ m}^{-1}$ (for both orientations of $\mathbf{b} = \pm b\hat{y}$ in the sample). From these curves one can read off the maximum possible values of rectification in 4 cases: (a) $\eta = 8282$ for $b = 2 \times 10^8 \text{ m}^{-1}$ at a distance of $2.04 \mu\text{m}$ and

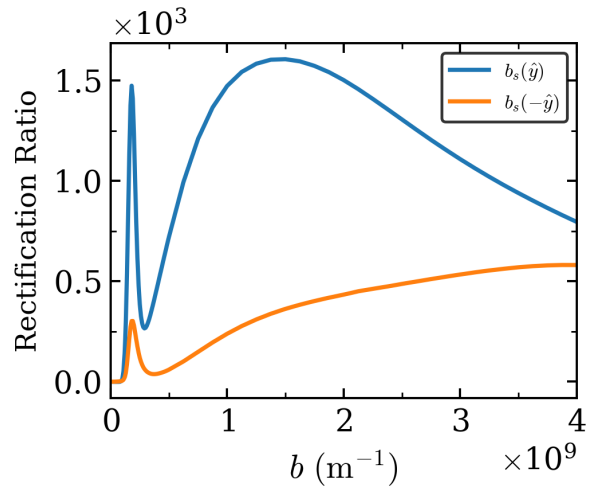


Figure 7: Rectification ratio η from Eq. (14) for $\mathbf{b} = b\hat{y}$ in the substrate in positive y direction and $\tilde{\eta}$ from Eq. (15) for $\mathbf{b} = -b\hat{y}$ in the substrate in negative y direction as a function of the Weyl node separation for the interparticle distance $d = 1000 \text{ nm}$. In the particles we have in both cases $\mathbf{b} = b\hat{y}$.

(b) $\eta = 5498$ for $b = 2 \times 10^9 \text{ m}^{-1}$ at a distance of $1.9 \mu\text{m}$ both when the orientation of the Weyl node separation is $\mathbf{b} = b\hat{y}$, and (c) $\tilde{\eta} = 292$ for $b = 2 \times 10^8 \text{ m}^{-1}$ at a distance of $1.14 \mu\text{m}$, and (d) $\tilde{\eta} = 895$ for $b = 2 \times 10^9 \text{ m}^{-1}$ at a distance of $1.6 \mu\text{m}$ both when the orientation of the Weyl node separation in the substrate is $\mathbf{b} = -b\hat{y}$. Hence, by turning the sample by 180° it is possible to inverse the direction of the preferred heat flow with still substantial rectification ratios.

VI. CONCLUSION

We have studied the rectification of thermal radiation between two WSM nanoparticles in the vicinity of a planar WSM sample in Voigt configuration. We have shown that the rectification direction and amplitude highly depends on the coupling of the localized nanoparticle resonances to the non-reciprocal surface modes of the planar substrate. We find extremely large rectification ratios in backward direction with values of $\eta \approx 5000 - 8530$ for the studied parameters. These values are much higher than previously predicted values for the same configuration of 2673. The rectification can be understood qualitatively and quantitatively by the properties of the surface modes and the coupling to either surface modes propagating in forward or backward direction. We highlight that the rectification in forward direction with ratios $\tilde{\eta} \approx 4 - 15$ for very small values of $b < 10^8 \text{ m}^{-1}$ as well as the huge backward rectification $\eta \approx 8300$ for values of $b \approx 2 \times 10^8 \text{ m}^{-1}$ have been overlooked in previous works. This finding might open interesting possibilities for heat flux rectification for WSM with small Weyl node separation. On the other hand, for values of $b = 2 \times 10^9 \text{ m}^{-1}$

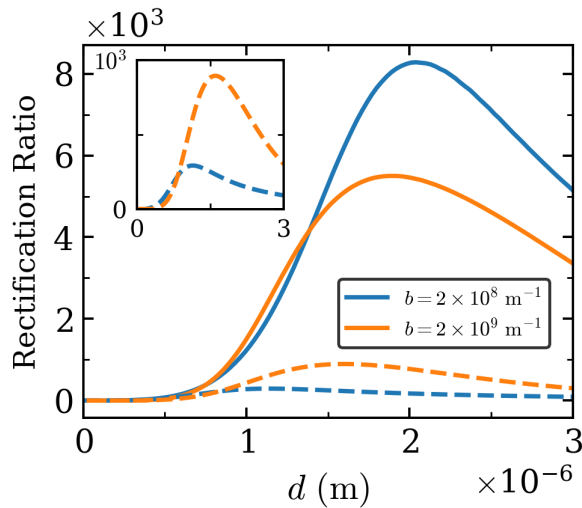


Figure 8: Rectification ratio η (solid line) from Eq. (14) as function of distance d for or $b = 2 \times 10^8 \text{ m}^{-1}$ and or $b = 2 \times 10^9 \text{ m}^{-1}$ as well as $\tilde{\eta}$ (dashed line) from Eq. (15) for $\mathbf{b} = -b\hat{y}$ in the substrate, i.e. the substrate is rotated by 180° , for $b = 2 \times 10^8 \text{ m}^{-1}$ and $b = 2 \times 10^9 \text{ m}^{-1}$. Inset: Shows a blow up of the rectification ratios $\tilde{\eta}$.

as found Co_3MnGa and Co_2MnGa we find a large rectification in backward direction only. Even though b cannot be modified in WSM there are other WSM with similar parameters Co_3MnGa and Co_2MnGa but with smaller values of b like $\text{Co}_3\text{Sn}_2\text{S}_2$, for instance. By turning the sample the directionality can be inverted but the coupling to the surface modes will be reduced so that a rectification in forward direction can be obtained which is much smaller than the rectification in backward direction but with a rectification ratios up to about 300-900 which are still very substantial compared to the rectification ratio of 249 reported for InSb with applied magnetic fields [28].

Acknowledgements

The authors gratefully acknowledge financial support from the Niedersächsische Ministerium für Kultur und Wissenschaft ('DyNano') and discussions with Achim Kittel.

-
- [1] C. R. Otey, W. T. Lau, and S. Fan, Thermal Rectification through Vacuum, *Phys. Rev. Lett.* **104**, 154301 (2010).
 - [2] H. Iizuka and S. Fan, Rectification of evanescent heat transfer between dielectric-coated and uncoated silicon carbide plates, *J. Appl. Phys.* **112**, 024304 (2012).
 - [3] S. Basu and M. Francoeur, Near-field radiative transfer based thermal rectification using doped silicon, *Appl. Phys. Lett.* **95** 231913 (2011).
 - [4] L. P. Wang and Z. M. Zhang, Thermal rectification enabled by near-field radiative heat transfer between intrinsic silicon and a dissimilar material, *Nanoscale and Microscale Thermophysical Engineering* **17**, 337(2013).
 - [5] E. Nefzaoui, K. Joulain, J. Drevillon, and Y. Ezzahri, Radiative thermal rectification using superconducting materials, *Appl. Phys. Lett.* **104**, 103905 (2014).
 - [6] J. Ordonez-Miranda, K. Joulain, D. De Sousa Menezes, Y. Ezzahri, and J. Drevillon, Photonic thermal diode based on superconductors, *J. Appl. Phys.* **112**, 093105 (2017).
 - [7] P. Ben-Abdallah and S.-A. Biehs, Phase-change radiative thermal diode, *Appl. Phys. Lett.* **103**, 191907 (2013).
 - [8] Y. Yang, S. Basu, L. Wang, Radiation-based near-field thermal rectification with phase transition materials, *Appl. Phys. Lett.* **103**, 163101 (2013).
 - [9] K. Ito, K. Nishikawa, H. Iizuka, and H. Toshiyoshi, Experimental investigation of radiative thermal rectifier using vanadium dioxide, *Appl. Phys. Lett.* **105** 25350 (2014).
 - [10] A. Fiorino, D. Thompson, L. Zhu, R. Mittapally, S.-A. Biehs, O. Bezencenet, N. El-Bondry, S. Bansropun, P. Ben-Abdallah, E. Meyhofer, P. Reddy, A thermal diode based on nanoscale thermal radiation, *ACS Nano* **12**, 5774 (2018).
 - [11] P. Ben-Abdallah and S.-A. Biehs, Near-field thermal transistor, *Phys. Rev. Lett.* **112**, 044301 (2014).
 - [12] Y. Li, Y. Dang, S. Zhang, X. Li, Y. Jin, P. Ben-Abdallah, J. Xu, and Y. Ma, Radiative thermal transistor, *Phys. Rev. Appl.* **20**, 024061 (2023).
 - [13] I. Latella, P. Ben-Abdallah, and M. Nikbakht, Radiative thermal rectification in many-body systems, *Phys. Rev. B* **104**, 045410 (2021).
 - [14] L. Zhu, S. Fan, Persistent directional current at equilibrium in nonreciprocal many-body near field electromagnetic heat transfer, *Phys. Rev. Lett.* **117**, 134303 (2016).
 - [15] A. Ott, P. Ben-Abdallah, and S.-A. Biehs, Circular heat and momentum flux radiated by magneto-optical nanoparticles, in *Phys. Rev. B* **97**, 205414 (2018).
 - [16] M. G. Silveirinha, Topological angular momentum and radiative heat transport in closed orbits, *Phys. Rev. B* **95**, 115103 (2017).
 - [17] P. Ben-Abdallah, Photon Thermal Hall Effect, *Phys. Rev. Lett.* **116**, 084301 (2016).
 - [18] J. Dong, W. Zhang, L. Liu, Nonreciprocal thermal radiation of nanoparticles via spin-directional coupling with reciprocal surface modes, *Appl. Phys. Lett.* **119**, 021104 (2021).
 - [19] I. Latella and P. Ben-Abdallah, Giant thermal magnetoresistance in plasmonic structures, *Phys. Rev. Lett.* **118**, 173902, (2017).
 - [20] R. M. Abraham Ekeroth, P. Ben-Abdallah, J.C. Cuevas, and A. Garcia Martin, Anisotropic thermal magnetoresistance for an active control of radiative heat transfer, *ACS Photonics* **5**, 705 (2017).
 - [21] S.-A. Biehs and P. Ben-Abdallah, Heat transfer mediated by the Berry phase in nonreciprocal many-body systems, *Phys. Rev. B* **106**, 235412(2022).

- [22] F. Herz, S.-A. Biehs, Green-Kubo relation for thermal radiation in non-reciprocal systems, *EPL* **127**, 4 (2019).
- [23] E. Moncada-Villa, V. Fernández-Hurtado, F.J. Garcia-Vidal, A. García-Martín, J. C. Cuevas, Magnetic field control of near-field radiative heat transfer and the realization of highly tunable hyperbolic thermal emitters, *Phys. Rev. B* **92**, 125418 (2015).
- [24] Lei Qu, Svend-Age Biehs, and Hong-Liang Yi, Extremely large thermal magnetoresistance and magnetic-field-driven transport-regime transition in macroscopic magneto-optical many-body systems, *Phys. Rev. Applied* **21**, 064022 (2024).
- [25] L. Fan, Y. Guo, G.T. Papadakis, B. Zhao, Z. Zhao, S. Buddhiraju, M. Orenstein, S. Fan, Nonreciprocal radiative heat transfer between two planar bodies, *Phys. Rev. B* **101**, 085407 (2020).
- [26] S. G. Castillo-Lopez, A. Marquez, and R. Esquivel-Sirvent, Resonant enhancement of the near-field radiative heat transfer in nanoparticles, *Phys. Rev. B* **105**, 155404 (2020).
- [27] A. Ott, R. Messina, P. Ben-Abdallah, and S. A. Biehs, Radiative thermal diode driven by nonreciprocal surface waves, *Appl. Phys. Lett.* **114**, 163105 (2019).
- [28] A. Ott and S. A. Biehs, Thermal rectification and spin-spin coupling of nonreciprocal localized and surface modes, *Phys. Rev. B* **101**, 155428 (2020).
- [29] T. Van Mechelen, Z. Jacob, Universal spin-momentum locking of evanescent waves, *Optica* **3**, 118 (2016).
- [30] C. Khandekar, Z. Jacob, Thermal spin photonics in the near-field of nonreciprocal media, *New J. Phys.* **21**, 103030 (2019).
- [31] S. A. Biehs, R. S. Messina, P. Venkataram, A. W. Rodriguez, J. C. Cuevas, and P. Ben-Abdallah, Near-field radiative heat transfer in many-body systems, *Rev. Mod. Phys.* **93**, 025009 (2021).
- [32] A. Ott, R. Messina, P. Ben-Abdallah, S.-A. Biehs, Magnetothermoplasmonics: from theory to applications, *J. Photon. Energy* **9**, 032711 (2019).
- [33] Q. Chen, A.R. Kutayiah, I. Oladyshkin, M. Tokman, A. Belyanin, Optical properties and electromagnetic modes of Weyl semimetals, *Phys. Rev. B* **99**, 075137 (2019).
- [34] O.V. Kotov, Y.E. Lozovik, Giant tunable nonreciprocity of light in Weyl semimetals, *Phys. Rev. B* **98**, 195446 (2018).
- [35] H. Da, Q. Song, H. Ye, X. Yan, Nonreciprocal photonic spin hall effect of magnetic Weyl semimetals, *Appl. Phys. Lett.* **119**, 081103 (2021).
- [36] A. Ott, S.-A. Biehs, and P. Ben-Abdallah, Anomalous photon thermal Hall effect, *Phys. Rev. B* **101**, 241411(R) (2020).
- [37] G. Xu, J. Sun, H. Mao, Near-field radiative thermal modulation between Weyl semimetal slabs, *J. Quant. Spectrosc. Radiat. Transf.* **253**, 107173 (2020).
- [38] Z. Yu, X. Li, T. Lee, H. Iizuka, Near-field radiative heat transfer between Weyl semimetal multilayers, *Int. J. Heat Mass Transf.* **197**, 123339 (2022).
- [39] G. Tang, J. Chen, L. Zhang, Twist-induced control of near-field heat radiation between magnetic Weyl semimetals, *ACS Photonics* **8**, 443 (2021).
- [40] Z. Yu, X. Li, T. Lee, H. Iizuka, Near-field radiative heat transfer in three-body Weyl semimetals, *Opt. Express* **30**, 31584 (2022).
- [41] Y. Sheng, Optimization of a Weyl-semimetal-based near-field heat transfer system, *Int. Comm. Heat Mass Transf.* **149**, 107137 (2023).
- [42] Y. Sun, Y. Hu, K. Shi, J. Zhang, D. Feng, X. Wu, Negative differential thermal conductance between Weyl semimetals nanoparticles through vacuum, *Physica Scripta* **97**, 095506 (2022).
- [43] C. Guo, B. Zhao, D. Huang, S. Fan, Radiative thermal router based on tunable magnetic Weyl semimetals, *ACS Photonics* **7**, 3257 (2020).
- [44] B. Zhao, C. Guo, C.A.C. Garcia, P. Narang, S. Fan, Axion-field-enabled nonreciprocal thermal radiation in Weyl semimetals, *Nano Lett.* **20**, 1923 (2020).
- [45] Z. Zhang and L. Zhu, Broadband Nonreciprocal Thermal Emission, *Phys. Rev. Appl.* **19**, 014013 (2023).
- [46] Y. Wang, C. Khandekar, X. Gao, T. Li, D. Jiao, Z. Jacob, Broadband circularly polarized thermal radiation from magnetic Weyl semimetals, *Opt. Mat. Expr.* **11**, 3880 (2021).
- [47] J. Wu and Y. M. Qing, Strong nonreciprocal radiation with topological photonic crystal heterostructure, *Appl. Phys. Lett.* **121**, 112201 (2022).
- [48] Z. Yu, X. Li, T. Lee, H. Iizuka, Nonreciprocal radiative heat transfer between Weyl semimetal nanoparticles mediated by graphene nanoribbons, *Int. J. Heat Mass Transf.* **214**, 124339 (2023).
- [49] C. Guo, V. S. Asadchy, B. Zhao, S. Fan, Light control with Weyl semimetals, *eLight* **3**, 2 (2023).
- [50] A. Didari-Bader, S. Kim, H. Choi, S. Seo, P. Biswas, H. Jeong, C.-W. Lee, Topological materials for near-field radiative heat transfer, *Mat. Today Phys.* **46**, 101489 (2024).
- [51] Y. Hu, H. Liu, B. Yang, K. Shi, M. Antezza, X. Wu, and Y. Sun, High-rectification near-field radiative thermal diode using Weyl semimetals, *Phys. Rev. Mat.* **7**, 035201 (2023).
- [52] K. Sääskilähti, J. Oksanen, J. Tulkki, Quantum Langevin equation approach to electromagnetic energy transfer between dielectric bodies in an inhomogeneous environment, *Phys. Rev. B* **89**, 134301 (2014).
- [53] K. Asheichyk, B. Müller, M. Krüger, Heat radiation and transfer for point particles in arbitrary geometries, *Phys. Rev. B* **96**, 155402 (2017).
- [54] J. Dong, J. Zhan, and L. Liu, Long-distance near-field energy transport via propagating surface waves, *Phys. Rev. B* **97**, 075422 (2018).
- [55] R. Messina, S.-A. Biehs, and P. Ben-Abdallah, Surface-mode-assisted amplification of radiative heat transfer between nanoparticles, *Phys. Rev. B* **97**, 165437 (2018).
- [56] Y. Zhang, M. Antezza, H.-L. Yi, H.-P. Tan, Metasurface-mediated anisotropic radiative heat transfer between nanoparticles, *Phys. Rev. B* **100**, 085426 (2019).
- [57] M.-J. He, H. Qi, Y.-T. Ren, Y.-J. Zhao, M. Antezza, Graphene-based thermal repeater, *Appl. Phys. Lett.* **115**, 263101 (2019).
- [58] B. Liu, M. Luo, J. Zhao, L. Liu, M. Antezza, Many-body interaction on near-field radiative heat transfer between two nanoparticles caused by proximate particle ensembles, *Int. J. Heat and Mass Transf.* **215**, 124462 (2023).
- [59] A. Narayanaswamy and G. Chen, Thermal near-field radiative transfer between two spheres, *Phys. Rev. B* **77**, 075125 (2008).
- [60] C. Otey, S. Fan, Numerically exact calculation of electromagnetic heat transfer between a dielectric sphere and plate, *Phys. Rev. B* **84**, 245431 (2011).
- [61] D. Becerril, C. Noguez, Near-field energy transfer be-

- tween nanoparticles modulated by coupled multipolar modes, *Phys. Rev. B* **99**, 045418 (2019).
- [62] A. Marquez and R. Esquivel-Sirvent, Terahertz response of plasmonic nanoparticles: Plasmonic Zeeman Effect, *Opt. Expr.* **28**, 39005 (2020).
- [63] J. Hofmann and S. Das Sarma, Surface plasmon polaritons in topological Weyl semimetals, *Phys. Rev. B* **93** 241402(R) (2016).
- [64] J.J. Brion, R. F. Wallis, A. Hartstein, E. Burstein, Theory of surface magnetoplasmons in semiconductors, *Physical Review Letters* **28**, 1455 (1972).
- [65] R. Wallis, J. Brion, E. Burstein and A. Hartstein, Theory of surface polaritons in anisotropic dielectric media with application to surface magnetoplasmons in semiconductors, *Phys. Rev. B*, **9**,8 (1974).
- [66] K. Chiu and J. Quinn. Magneto-plasma surface waves in solids, *Nuovo Cimento B* **10**,1 (1972).
- [67] H. C. Chen, A coordinate-free approach to wave reflection from an anisotropic medium, *Radio Science* **16**, 1213 (1981).